의학석사 학위논문

Serial IV Contrast-Enhanced T1 Mapping for Quantitative Evaluation of Dynamic Glymphatic Activity: Feasibility Study

동적 글림프계 활성도의 정량적 평가를 위한 연쇄적 정맥 조영 증강 T1 맵핑: 타당성 연구

2020 년 08 월

서울대학교 대학원

의학과 영상의학 전공

이 상 협

Abstract

Serial IV Contrast-Enhanced T1 Mapping for Quantitative Evaluation of Dynamic Glymphatic Activity: Feasibility Study

Sanghyup Lee

Department of Radiology, College of Medicine

The Graduate School

Seoul National University

Background: Glymphatic system is a glial-dependent waste clearance pathway which increases in activity at night. Evaluation of the glymphatic system with dynamic MR imaging after intrathecal contrast injection has limited clinical use.

Purpose: To investigate the feasibility of using serial IV contrast-enhanced T1 mapping for quantitative evaluation of dynamic glymphatic activity in various anatomical locations in healthy subjects.

Materials and Methods: In this prospective study with a randomized, 2-way crossover design, 25 healthy participants in the age of 20s

(mean age, 24.7 years; range, 23–29; 15 men and 10 women) underwent two cycles of contrast-enhanced MR imaging (day and night cycles), separated by a period of 1 week, between May 2019 and February 2020. For each cycle, MR scans (3D T1-weighted images and T1 maps) were acquired at baseline and 0.5, 1, 1.5, 2, and 12 hours after IV contrast injection. The time (t_{min}) to reach the minimum T1 value ($T1_{min}$), absolute difference between the precontrast T1 and $T1_{min}$ (peak ΔT1), slope between two measurements at 2 hours and 12 hours post-injection ($slope_{[2h-12h]}$) were calculated on T1 value-time curves at cerebral GM/WM, cerebellar GM/WM, and putamen. Mixed model analysis of variance (ANOVA) was performed to assess the effect of sleep on $slope_{[2h-12h]}$. Friedman test and repeated-measures ANOVA were performed to compare t_{min} and peak ΔT1 among different anatomical locations, respectively.

Results: All T1 value-time curves showed the initial decrease at 0.5 hours post-injection followed by gradual recovery up to 12 hours. $Slope_{[2h-12h]}$ increased from day to night at the cerebral GM, cerebellar GM, and putamen (P<.001 for all) but not at the cerebral

WM (P=1.00) and cerebellar WM (P=.42). Median t_{min} values were 0.5 h at the cerebral GM, cerebellar GM, and putamen for both cycles. Cerebellar GM had the highest peak ΔT1 (mean±standard deviation, 158.89msec±5.76[day], 151.57msec±6.43[night]), followed by cerebral GM (99.36msec±4.45, 104.34msec±5.46), and putamen (62.25 msec±4.64, 57.94msec±4.24).

Conclusion: Change in T1 values at the cerebral/cerebellar GMs and putamen on serial IV contrast-enhanced T1 maps may serve as a potential imaging biomarker for dynamic glymphatic activity.

Keywords: Glymphatic system, quantification, IV contrast-enhanced T1 mapping, T1 value

Student Number: 2018-23561

Table of contents

List of tables

List of figures

Introduction

The glymphatic system, glial-dependent waste clearance pathway for soluble proteins and metabolites, is an emerging circulatory model in the brain, characteristically devoid of authentic lymphatic vessels. The key component of the glymphatic system is the perivascular space, where the cerebrospinal fluid (CSF) is allowed to enter the interstitial space of the brain parenchyma through the aquaporin-4 (AQP4) water channels at the end feet of astrocytes (1). CSF mixed with the interstitial fluid then exits the brain via the perivenous space along with metabolic waste products released from cells. Waste clearance pathway downstream to the glymphatic system comprises meningeal lymphatic vessels, authentic lymphatic network found at the dura, cranial nerves, and large vessels at the skull exits (2).

Given the accumulating evidence from previous preclinical studies suggesting the clearance of metabolites such as tau protein, amyloid-β, and lactate from the brain through the glymphatic system (1, 3, 4), impairment of the glymphatic system has been highlighted as the important pathophysiology of various pathologic conditions, including

Alzheimer's disease, traumatic brain injury (TBI), and normal pressure hydrocephalus (NPH) (5-8).

Over the past few years, several preclinical studies have demonstrated the glymphatic activity using fluorescent CSF tracers. The influx and clearance of fluorescent CSF tracers injected into the intrathecal and intracisternal spaces of rats and mice have been measured for dynamic evaluation of glymphatic activity (7, 9). Alternatively, dynamic MR imaging using gadolinium-based contrast agents (GBCAs) has also been studied as a potential tool to assess the glymphatic activity. Iliff et al. observed that intrathecally injected GBCA entered the brain along the perivascular pathways in rats (10). Jost et al. performed repeated fluid attenuated MRI after high-dose intravenous (IV) administration of various GBCAs to rats, evaluating the penetration of GBCAs from the blood into the CSF and their distribution kinetics within different CSF cavities (11). Of note, a close association between sleep and the glymphatic activity has also been reported in the previous study that investigated the tissue gadolinium concentration after IV injection of linear GBCA at varying time in rats (12). In humans, the glymphatic activity at different brain anatomical regions has been assessed by

measuring the signal intensity change over time on 3D T1-weighted gradient echo (8, 13-15) or T1 mapping (16) after intrathecal injection of GBCA. Moreover, the influx of intravenously injected GBCA into the perivascular space has also been depicted on heavily T2-weighted 3D-fluid attenuated inversion recovery (FLAIR) images 4 hours after the injection (17).

To our knowledge, however, there has been no study that analyzed the glymphatic activity in the brain by means of dynamic MR imaging after IV administration of GBCA. Therefore, we aimed to investigate the feasibility of using serial IV contrast-enhanced T1 mapping for quantitative evaluation of dynamic glymphatic activity in various anatomical locations in healthy subjects. We hypothesized that change in T1 value due to the glymphatic activity would be more pronounced in the cortex or deep gray matter (GM) with prominent perivascular space than in white matter (WM), and are more evident at night than during the day (18).

Materials and Methods

This prospective study was approved by the institutional review board of the Seoul National University Hospital (IRB No. 1811-164-992) and written informed consent was obtained from all patients.

Study Design and Study Population

This investigation was based on a single center, randomized, 2-way crossover study design. Each participant underwent two contrast-enhanced MR imaging periods, separated by a washout period of 1 week to minimize the carryover effect. For each period, MR scans were acquired at baseline (precontrast), and after IV injection of GBCA. For the postcontrast MR imaging, 4 serial MR images were acquired during the first 2 hours at a 30-minute interval (0.5, 1, 1.5, and 2 hours after the contrast injection), followed by the final delayed acquisition at 12 hours. For the day cycle without sleep, the precontrast images were acquired at 8:30 AM. Following the IV injection of GBCA at 9:00 AM, 4 serial MR images were acquired at a 30-minute interval starting from 9:30 AM with the final delayed images acquired at 9:00 PM. During the day cycle, the

subjects were not restricted in their daily activities including meals, but were strictly informed so as not to sleep at all before the final image acquisition. For the night cycle with sleep, the precontrast images were acquired at 8:30 PM. Following the IV injection of GBCA at 9:00 PM, 4 serial MR images were acquired at a 30-minute interval starting from 9:30 PM. The participants returned home to have normal night's sleep before being scanned for the final delayed images at 9:00 AM the next morning.

Participants were healthy volunteers enrolled from May 2019 to February 2020, meeting the following inclusion criteria: 1) an age of 20 to 30 years regardless of gender and 2) no history of any kind of neurological disease or traumatic brain injury. Exclusion criteria were as follows: 1) any contraindication to the MR imaging, such as cardiac pacemaker implanted state or claustrophobia; 2) any contraindication to the use of GBCA, such as renal failure or past history of adverse reaction to GBCA; and 3) incidentally detected brain lesion on MR imaging. Target ample size was calculated by reference from a calculation method in bioequivalence studies, which typically use the 2x2 crossover design (19). With the significance level $\alpha = 0.05$ and desired power = 0.9, a total

number of 22 participants were the minimal requirement for verifying any difference between the day and night cycles (19). Considering potential dropouts during the study period, a total of 32 volunteers were recruited and there was no participant who has been reported in other prior studies. Four of them declined to participate during the study schedule coordination process. The remaining 28 participants were randomized into two groups starting the first period either with the day (group A) or night (group B) cycle. After a week of washout for every participant, they crossed over to the second period by switching the day and night cycles. During the first period, 3 participants (2 from group A, 1 from group B) were excluded from the study. One in the group A complained of claustrophobia, and the other participant declined to participate due to headache and fatigue during the first period. One participant in the group B was excluded because of MR machine error during the dynamic image acquisition. The final study population included 25 participants (Fig 1).

MRI Protocol

All study participants underwent MRI studies using a 3.0-T imaging unit (TrioTim, Siemens Healthineers, Erlangen, Germany) with a 32-channel

head coil. The MR imaging protocol included pre- and serial dynamic postcontrast three-dimensional fast spoiled gradient echo (3D FSPGR) sequences with multiplanar reconstructions of the sagittal, coronal, and transverse T1-weighted images, and T1 mapping using a magnetization prepared 2 rapid acquisition gradient echoes (MP2RAGE) sequence (20). The IV GBCA bolus injection was manually done at the right median antecubital vein, using gadobutrol (Gadovist; Bayer Schering Pharma, Berlin, Germany) at a dose of 0.1 mmol/kg of body weight. Specific imaging parameters for all sequences are provided in Table E1.

Phantom Calibration Study

Phantom calibration study was performed to validate the intra-scanner variability of T1 values measured with the MP2RAGE sequence. The methods and results are summarized in Appendix E1, Table E2, and Fig E1.

MRI Analysis

All image analyses were performed by one radiologist (S.H.L., with 4 years of brain MRI experience in training), who was blinded to the group

information of each participant, under the supervision of an expert neuroradiologist (R.E.Y., with 10 years of experience in neuroradiology). Default settings of the open-source software (FreeSurfer, version 6.0.0; Laboratory for Computational Neuroimaging, Boston, Mass) were used to perform automatic cortical reconstruction and volumetric segmentation based on the 3D T1-weighted images as described in previous studies (21-26). The technical details of these procedures are described in prior publications (27-31), and our study participants' images were registered to a Destrieux atlas embedded in the FreeSurfer (32). The masks were selected at the various anatomical locations, including bilateral cerebral GM, cerebral WM, cerebellar GM, cerebellar WM, and putamen. The T1 mapping data from MP2RAGE sequence were processed on a dedicated commercial software package (NordicICE, version 4.1.2; NordicNeuroLab, Bergen, Norway). Coregistration between the brain region masks and the T1 maps was performed using the software, with automatic correction of the difference in section thickness between images. After the automatic coregistration, the data were manually inspected and minimally edited for detailed anatomical corrections, if needed. T1 values were determined on a pixel-by-pixel basis for the

total volumes of interest defined by the auto-segmented mask, and the mean T1 value of each mask was calculated for baseline and multiple time points after the contrast injection (Fig 2). Subsequently, changes in individual and mean T1 values from baseline at various anatomical locations over time were plotted for each cycle, and the minimum T1 value ($T1_{min}$) and the time taken to reach $T1_{min}$ (t_{min}) were determined based on the visual inspection of T1 value-time curves. The absolute difference between the precontrast T1 value and $T1_{min}$ values (peak $\Delta T1$) was calculated for each cycle to reflect the initial influx of the contrast agent by the glymphatic system. Furthermore, the slope between two measurements at 2 hours and 12 hours after the contrast injection ($slope_{[2h-12h]}$) was calculated for each cycle to account for delayed clearance of the contrast agent.

Statistical Analysis

All statistical analyses were performed using the statistical software MedCalc, version 19.2.0 (MedCalc, Mariakerke, Belgium). Normality of the data for each parameter was assessed using the Kolmogorov-Smirnov test. Non-parametric data are reported as the median and interquartile

range (IQR) while parametric data are presented as the mean ± standard deviation. Intra-scanner variability of T1 values for the phantom calibration study was assessed using the intraclass correlation coefficient: 0.00–0.20, slight agreement; 0.21–0.40, fair agreement; 0.41–0.60, moderate agreement; 0.61–0.80, substantial agreement; and 0.81–1.00, almost perfect agreement (33). To analyze the effect of sleep on the glymphatic activity, the log-transformed $slope_{[2h-12h]}$ was compared between day and night cycles using mixed model analysis of variance (ANOVA) for a 2 × 2 crossover design, controlling for the sequence of MR acquisition (i.e., group A: day cycle [1st period] → night cycle [2nd period]; group B: night cycle [1st period] → day cycle [2nd period]). Friedman test and repeated-measures analysis of variance (RM-ANOVA), followed by post hoc tests with Bonferroni correction for multiple comparisons, were performed to assess the difference in t_{min} and peak ΔT1 values among the different anatomical locations, respectively. *P* values less than .05 were considered to be statistically significant in all tests.

Results

Study Participant Characteristics

A total of 25 participants (mean age, 24.7 years; range, 23–29; 15 men and 10 women) were evaluated. Group A (day cycle [1st period] → night cycle [2nd period]) included 12 participants (mean age, 25.3 years; range, 23–29 years; 6 men and 6 women) while group B (night cycle [1st period] → day cycle [2nd period]) included 13 participants (mean age, 24.2 years; range, 23–27 years; 9 men and 4 women).

Phantom Calibration Study

Intraclass correlation coefficient for repeated measurements of T1 values on the phantom study was excellent (ICC; 0.999, 95% confidence interval [CI]; 0.994 – 1.000).

Comparison of T1 Value–Time Curves

The graphs plotting the mean T1 values over time for various anatomical locations showed a common pattern characterized by the initial rapid decrease followed by gradual recovery in general, but the magnitude of

changes was different according to the anatomical locations and cycles (Fig 3).

Comparison of slope$_{[2h-12h]}$ between day and night cycles for each anatomical location

Slope$_{[2h-12h]}$ values significantly increased from day to night at the cerebral GM, cerebellar GM, and putamen (Geometric mean ratio (Night/Day); 1.41, 2.07, and 2.37, respectively; $P < .001$ for all) but there was no significant difference between day and night in the cerebral WM and cerebellar WM (Geometric mean ratio (Night/Day); 0.01 and 2.36, respectively; $P = 1.00$ and 0.42) (Table 1, Fig 3). The effect of period and sequence for the mixed model was not statistically significant ($P > .05$).

Comparison of t_{min} and peak ΔT1 values between different anatomical locations

The t_{min} of day cycle was significantly shorter in the cerebral GM and putamen (median, 0.5 h for both locations) than in the cerebellar WM

(median, 1.25 h) (adjusted $P < .05$), but the t_{min} of night cycle was not significantly different among the anatomical locations ($P = .36$) (Table 2).

The peak ΔT1 values decreased in the following order for the day cycle: cerebellar GM (mean ± standard deviation, 158.89 msec ± 5.76), cerebral GM (99.36 msec ± 4.45), putamen (62.25 msec ± 4.64), cerebellar WM (61.92 msec ± 11.58), and cerebral WM (54.84 msec ± 11.13). Statistical significance was found in all pairwise comparisons (adjusted P value < .05) except for cerebral WM vs. cerebellar WM, cerebral WM vs. putamen, and cerebellar WM vs. putamen ($P = 1.00$). The similar pattern was shown for the night cycle with the mean peak ΔT1 values decreasing in the following order: cerebellar GM (151.57 msec ± 6.43), cerebral GM (104.34 msec ± 5.46), putamen (57.94 msec ± 4.24), cerebral WM (52.24 msec ± 9.38), and cerebellar WM (33.90 msec ± 7.23). Statistical significance was found in all pairwise comparisons (adjusted P value < .05) except for cerebral WM vs. cerebellar WM ($P = 1.00$) and cerebral WM vs. putamen ($P = .72$) (Fig 4, Table E3).

Discussion

In this study, we investigated the feasibility of using the serial T1 mapping after IV injection of GBCA for quantitative evaluation of dynamic glymphatic activity. Key findings of this study were as follows: (a) T1 value–time curves at various anatomical locations showed a common pattern characterized by the initial rapid decrease followed by gradual recovery; (b) $slope_{[2h-12h]}$ values increased from day to night at the cerebral GM, cerebellar GM, and putamen, reflecting enhancement of delayed clearance of the contrast agent by the glymphatic system at night; (c) median t_{min} values were 0.5 h at the cerebral GM, cerebellar GM, and putamen; and (d) cerebellar GM had the highest peak ΔT1, followed by cerebral GM, and putamen.

In the glymphatic system, AQP4 water channels at the end feet of astrocytes (outer wall of the perivascular space) provide fast water transportation and play a pivotal role for the entrance of CSF into the interstitium of the brain tissue. Following the CSF influx, convection is known to be responsible for the subsequent CSF movement within the interstitium, where CSF exchanges with the interstitial fluid, collecting waste products from the tissue . Perivascular spaces are known to be most

prevalent along the lenticulostriate arteries entering the basal ganglia and perforating medullary arteries entering the high convexity cortical GM (34). Initial rapid decrease (with the t_{min} of 0.5 h) observed at the cerebral GM, cerebellar GM, and putamen is likely due to the CSF influx at the perivascular space in the glymphatic system, whereas the gradual recovery up to 12 hours post-injection may be attributable to the relatively slow efflux of the GBCA from the structures by convection. Our finding is consistent with that of the previous study on dynamic MR imaging after IV injection, in which the change in T1 signal to noise ratio from baseline showed a mild increase shortly after the injection followed by a gradual decrease taking more than 3 hours in rats (12).

Sleep has been reported to have a positive influence on the glymphatic activity (4, 12, 35, 36). Taoka et al. quantified tissue gadolinium concentration following IV injection of linear GBCA at varying time and found that the gadolinium concentration was lowest in the groups injected in the morning (when rats are asleep) (12). Given the established relationship between sleep and the glymphatic activity, we also compared the slope$_{[2h-12h]}$ between day and night cycles at the cerebral GM, cerebellar GM, and putamen and found that GBCA that entered the brain

parenchyma was cleared out more rapidly in the night cycle with normal sleep, a finding in keeping with the results of other studies. Of note, our study has importance in that this increase of glymphatic activity during sleep was clearly evaluated by IV contrast enhanced MRI in humans with a crossover study design.

Nonetheless, it should be noted that some portions of small cortical vessels and perforating vessels inside the perivascular spaces are inevitably integrated into the volumes of interest, which must be considered important in this study setting using IV injection of GBCA. However, a study that measured serial T1 values over time at the superior and inferior sagittal sinus lumens revealed the time to peak IV concentration was only 2 minutes after IV bolus injection (37). In comparison, the T1 values at the cerebral GM, cerebellar GM, and putamen in our study reached the minimum at 0.5 hours and were recovered gradually over a 12-hour period. Moreover, $slope_{[2h-12h]}$ changes according to sleep-wake cycle cannot be explained by intravascular GBCA effect, and thus we speculate that the change in T1 values observed in this study would mainly reflect the glymphatic activity rather than vascular enhancement and washout.

With regard to the comparison of T1 value–time curves between the three anatomical locations, the location that showed most profound decrease of the T1 value (highest peak ΔT1) at the early phase and also the greatest recovery at the delayed phase was the cerebellar GM, followed by the cerebral GM and putamen. The same trend was observed in the previous study that explored percentage change in signal unit ratio at various time points after intrathecal injection of GBCA (14). Moreover, tissue gadolinium concentration following IV injection of linear GBCA tissue was measured to be higher in the cerebellum than in the cerebrum at the same injection protocols (12). We speculate that the contributing factors to the difference among the anatomical locations are the distribution of the perivascular space and AQP4 channels within the space. Specifically, AQP4 channel expression levels have been found to be the highest in the cerebellum and spinal cord gray matter, which may account for the highest glymphatic activity in the cerebellar GM (38).

Meanwhile, the cerebral and cerebellar WMs showed a relatively small fluctuation of T1 values, along with high variability of the individual data. More important, unlike the GMs and putamen, $slope_{[2h-12h]}$ did not significantly increase during sleep. Several studies that evaluated changes

in normalized T1 signals (8, 14) or T1 values (16) over time using intrathecally injected GBCA as the CSF tracer have shown centripetal influx of the tracer from the cortex to deeper brain regions. Given that only a small amount of GBCA enters the CSF space via blood–CSF barrier at the choroid plexus, the amount of GBCA that moved centripetally from the GMs and putamen to the deep WM structures might have been too small to be detected with the current method, which may explain our findings in the WMs. The findings are in agreement with those of the previous studies that also demonstrated the lack of penetration of CSF tracers to deep WM (10, 14). Taken together, these data indicate that the change in T1 values at the cortex or putamen may be a more suitable candidate for evaluating the glymphatic activity than that at WMs when using IV contrast–enhanced MR imaging.

In terms of clinical implications, our MR imaging protocol with IV injection of GBCA, which is far more common and less invasive route for GBCA administration, may be considered to be more practical than those with intrathecal injection of the contrast media in routine practice. The change in T1 values at the cortex or putamen may serve as a potential surrogate marker for the therapeutic response as well as disease severity

in various neurodegenerative disorders with impaired glymphatic activity —– for example, Alzheimer's disease with amyloid plaque deposition.

There are several limitations in our study. First, the participants consisted of only normal and young individuals with a narrow range of age distribution. In order to incorporate our study results into clinical settings, further studies are warranted on extended subject groups including patients with various underlying medical conditions and different age subgroups. Second, the time points we set for the serial MR imaging were insufficient to elicit detailed dynamic information of T1 value change over time. An imaging time interval shorter than 30 minutes would have been more helpful for the accurate acquisition of dynamic information. Nevertheless, the dynamic curves obtained in our study showed acceptable quality for evaluation. Also, the participants' discomfort from repetitive MR imaging also needed to be taken into consideration in the study design. In future studies using a similar approach, image acquisition time points may be adjusted based on our study results. Third, many unknown confounding factors that may potentially affect the glymphatic activity in daily lives were not strictly controlled for when evaluating the effect of sleep on the glymphatic clearance. All participants were not

controlled for daily lives including dietary habits, physical activities such as exercise, and amount of night sleep, and thus caution is needed in interpretating the $slope_{[2h-12h]}$ analysis.

In conclusion, serial IV contrast-enhanced T1 mapping could be performed for the quantitative evaluation of dynamic glymphatic activity in the brain. In particular, change in T1 values at the cerebral/cerebellar GMs and putamen on serial IV contrast-enhanced T1 maps may serve as a potential imaging biomarker for dynamic glymphatic activity.

References

1. Iliff JJ, Wang M, Liao Y, Plogg BA, Peng W, Gundersen GA, Benveniste H, Vates GE, Deane R, Goldman SA, Nagelhus EA, Nedergaard M. A paravascular pathway facilitates CSF flow through the brain parenchyma and the clearance of interstitial solutes, including amyloid beta. Science translational medicine 2012;4(147):147ra111. doi: 10.1126/scitranslmed.3003748

2. Benveniste H, Liu X, Koundal S, Sanggaard S, Lee H, Wardlaw J. The Glymphatic System and Waste Clearance with Brain Aging: A Review. Gerontology 2019;65(2):106-119. doi: 10.1159/000490349

3. Patel TK, Habimana-Griffin L, Gao X, Xu B, Achilefu S, Alitalo K, McKee CA, Sheehan PW, Musiek ES, Xiong C, Coble D, Holtzman DM. Dural lymphatics regulate clearance of extracellular tau from the CNS. Molecular neurodegeneration 2019;14(1):11. doi: 10.1186/s13024-019-0312-x

4. Lundgaard I, Lu ML, Yang E, Peng W, Mestre H, Hitomi E, Deane R, Nedergaard M. Glymphatic clearance controls state-dependent changes

in brain lactate concentration. Journal of cerebral blood flow and metabolism : official journal of the International Society of Cerebral Blood Flow and Metabolism 2017;37(6):2112-2124. doi: 10.1177/0271678x16661202

5. Tarasoff-Conway JM, Carare RO, Osorio RS, Glodzik L, Butler T, Fieremans E, Axel L, Rusinek H, Nicholson C, Zlokovic BV. Clearance systems in the brain—implications for Alzheimer disease. Nature Reviews Neurology 2015;11(8):457.

6. Peng W, Achariyar TM, Li B, Liao Y, Mestre H, Hitomi E, Regan S, Kasper T, Peng S, Ding F. Suppression of glymphatic fluid transport in a mouse model of Alzheimer's disease. Neurobiology of disease 2016;93:215-225.

7. Kress BT, Iliff JJ, Xia M, Wang M, Wei HS, Zeppenfeld D, Xie L, Kang H, Xu Q, Liew JA. Impairment of paravascular clearance pathways in the aging brain. Annals of neurology 2014;76(6):845-861.

8. Eide PK, Ringstad G. Delayed clearance of cerebrospinal fluid tracer from entorhinal cortex in idiopathic normal pressure hydrocephalus: A glymphatic magnetic resonance imaging study. Journal of cerebral blood flow and metabolism : official journal of the International Society of

Cerebral Blood Flow and Metabolism 2019;39(7):1355-1368. doi: 10.1177/0271678x18760974

9. Yang L, Kress BT, Weber HJ, Thiyagarajan M, Wang B, Deane R, Benveniste H, Iliff JJ, Nedergaard M. Evaluating glymphatic pathway function utilizing clinically relevant intrathecal infusion of CSF tracer. Journal of translational medicine 2013;11(1):107.

10. Iliff JJ, Lee H, Yu M, Feng T, Logan J, Nedergaard M, Benveniste H. Brain-wide pathway for waste clearance captured by contrast-enhanced MRI. The Journal of clinical investigation 2013;123(3):1299-1309.

11. Jost G, Frenzel T, Lohrke J, Lenhard DC, Naganawa S, Pietsch H. Penetration and distribution of gadolinium-based contrast agents into the cerebrospinal fluid in healthy rats: a potential pathway of entry into the brain tissue. European radiology 2017;27(7):2877-2885.

12. Taoka T, Jost G, Frenzel T, Naganawa S, Pietsch H. Impact of the Glymphatic System on the Kinetic and Distribution of Gadodiamide in the Rat Brain: Observations by Dynamic MRI and Effect of Circadian Rhythm on Tissue Gadolinium Concentrations. Invest Radiol 2018;53(9):529-534. doi: 10.1097/RLI.0000000000000473

13. Eide PK, Vatnehol SAS, Emblem KE, Ringstad G. Magnetic resonance

imaging provides evidence of glymphatic drainage from human brain to cervical lymph nodes. Scientific reports 2018;8(1):7194.

14. Ringstad G, Valnes LM, Dale AM, Pripp AH, Vatnehol S-AS, Emblem KE, Mardal K-A, Eide PK. Brain-wide glymphatic enhancement and clearance in humans assessed with MRI. JCI insight 2018;3(13).

15. Zhou Y, Cai J, Zhang W, Gong X, Yan S, Zhang K, Luo Z, Sun J, Jiang Q, Lou M. Impairment of the Glymphatic Pathway and Putative Meningeal Lymphatic Vessels in the Aging Human. Ann Neurol 2020;87(3):357-369. doi: 10.1002/ana.25670

16. Watts R, Steinklein JM, Waldman L, Zhou X, Filippi CG. Measuring Glymphatic Flow in Man Using Quantitative Contrast-Enhanced MRI. AJNR American journal of neuroradiology 2019;40(4):648-651. doi: 10.3174/ajnr.A5931

17. Naganawa S, Nakane T, Kawai H, Taoka T. Gd-based contrast enhancement of the perivascular spaces in the basal ganglia. Magnetic Resonance in Medical Sciences 2017;16(1):61-65.

18. Kwee RM, Kwee TC. Virchow-Robin spaces at MR imaging. Radiographics : a review publication of the Radiological Society of North America, Inc 2007;27(4):1071-1086. doi: 10.1148/rg.274065722

19. Ring A, Lang B, Kazaroho C, Labes D, Schall R, Schütz H. Sample size determination in bioequivalence studies using statistical assurance. British journal of clinical pharmacology 2019;85(10):2369-2377. doi: 10.1111/bcp.14055

20. Marques JP, Kober T, Krueger G, van der Zwaag W, Van de Moortele PF, Gruetter R. MP2RAGE, a self bias-field corrected sequence for improved segmentation and T1-mapping at high field. NeuroImage 2010;49(2):1271-1281. doi: 10.1016/j.neuroimage.2009.10.002

21. Dale AM, Fischl B, Sereno MI. Cortical surface-based analysis. I. Segmentation and surface reconstruction. NeuroImage 1999;9(2):179-194. doi: 10.1006/nimg.1998.0395

22. Fischl B, Salat DH, van der Kouwe AJ, Makris N, Segonne F, Quinn BT, Dale AM. Sequence-independent segmentation of magnetic resonance images. NeuroImage 2004;23 Suppl 1:S69-84. doi: 10.1016/j.neuroimage.2004.07.016

23. Zöllei L, Iglesias JE, Ou Y, Grant PE, Fischl BJapa. Infant FreeSurfer: An automated segmentation and surface extraction pipeline for T1-weighted neuroimaging data of infants 0-2 years. 2020.

24. Schoene-Bake JC, Keller SS, Niehusmann P, Volmering E, Elger C, Deppe M, Weber B. In vivo mapping of hippocampal subfields in mesial temporal lobe epilepsy: relation to histopathology. Human brain mapping 2014;35(9):4718-4728. doi: 10.1002/hbm.22506

25. Kim YS, Kim M, Choi SH, You SH, Yoo RE, Kang KM, Yun TJ, Lee ST, Moon J, Shin YW. Altered Vascular Permeability in Migraine-associated Brain Regions: Evaluation with Dynamic Contrast-enhanced MRI. Radiology 2019;292(3):713-720. doi: 10.1148/radiol.2019182566

26. de Flores R, La Joie R, Landeau B, Perrotin A, Mezenge F, de La Sayette V, Eustache F, Desgranges B, Chetelat G. Effects of age and Alzheimer's disease on hippocampal subfields: comparison between manual and FreeSurfer volumetry. Human brain mapping 2015;36(2):463-474. doi: 10.1002/hbm.22640

27. Reuter M, Rosas HD, Fischl B. Highly accurate inverse consistent registration: a robust approach. NeuroImage 2010;53(4):1181-1196. doi: 10.1016/j.neuroimage.2010.07.020

28. Reuter M, Tisdall MD, Qureshi A, Buckner RL, van der Kouwe AJW, Fischl B. Head motion during MRI acquisition reduces gray matter volume and thickness estimates. NeuroImage 2015;107:107-115. doi:

10.1016/j.neuroimage.2014.12.006

29. Fischl B, Salat DH, Busa E, Albert M, Dieterich M, Haselgrove C, van der Kouwe A, Killiany R, Kennedy D, Klaveness S, Montillo A, Makris N, Rosen B, Dale AM. Whole brain segmentation: automated labeling of neuroanatomical structures in the human brain. Neuron 2002;33(3):341-355. doi: 10.1016/s0896-6273(02)00569-x

30. Segonne F, Pacheco J, Fischl B. Geometrically accurate topology-correction of cortical surfaces using nonseparating loops. IEEE transactions on medical imaging 2007;26(4):518-529. doi: 10.1109/tmi.2006.887364

31. Fischl B, Dale AM. Measuring the thickness of the human cerebral cortex from magnetic resonance images. Proceedings of the National Academy of Sciences of the United States of America 2000;97(20):11050-11055. doi: 10.1073/pnas.200033797

32. Destrieux C, Fischl B, Dale A, Halgren E. Automatic parcellation of human cortical gyri and sulci using standard anatomical nomenclature. NeuroImage 2010;53(1):1-15. doi: 10.1016/j.neuroimage.2010.06.010

33. Landis JR, Koch GG. The measurement of observer agreement for categorical data. Biometrics 1977;33(1):159-174.

34. Heier LA, Bauer CJ, Schwartz L, Zimmerman RD, Morgello S, Deck MD. Large Virchow-Robin spaces: MR-clinical correlation. AJNR American journal of neuroradiology 1989;10(5):929-936.

35. Liu DX, He X, Wu D, Zhang Q, Yang C, Liang FY, He XF, Dai GY, Pei Z, Lan Y, Xu GQ. Continuous theta burst stimulation facilitates the clearance efficiency of the glymphatic pathway in a mouse model of sleep deprivation. Neuroscience letters 2017;653:189-194. doi: 10.1016/j.neulet.2017.05.064

36. Xie L, Kang H, Xu Q, Chen MJ, Liao Y, Thiyagarajan M, O'Donnell J, Christensen DJ, Nicholson C, Iliff JJ, Takano T, Deane R, Nedergaard M. Sleep drives metabolite clearance from the adult brain. Science (New York, NY) 2013;342(6156):373-377. doi: 10.1126/science.1241224

37. Taheri S, Shah NJ, Rosenberg GA. Analysis of pharmacokinetics of Gd-DTPA for dynamic contrast-enhanced magnetic resonance imaging. Magnetic resonance imaging 2016;34(7):1034-1040. doi: 10.1016/j.mri.2016.04.014

38. Hubbard JA, Hsu MS, Seldin MM, Binder DK. Expression of the Astrocyte Water Channel Aquaporin-4 in the Mouse Brain. ASN Neuro 2015;7(5). doi: 10.1177/1759091415605486

Tables

Table 1. Change in Slope$_{[2h-12h]}$ According to Day/Night Cycle at Each Anatomical Location

Location	Geometric Mean of Slope$_{[2h-12h]}$ (msec/h)		Geometric Mean Ratio (Night/Day)		
	Day	Night	Point estimate	95% Confidence interval	*P* Value
Cerebral GM	3.62	5.08	1.41	1.16, 1.71	.001
Cerebral WM	0.48	0.48	0.01	−3.58, 3.60	1.00
Cerebellar GM	7.95	9.97	2.07	1.14, 2.99	<.001
Cerebellar WM	−3.52	−1.15	2.36	−3.54, 8.26	.42
Putamen	1.55	3.66	2.37	1.55, 3.62	<.001

Note.—Mixed model analysis of variance was used to compare log−transformed slope$_{[2h-12h]}$ between day and night cycles. The Slope$_{[2h-12h]}$ was defined as the slope between two measurements at 2 hours and 12 hours after the contrast injection.

Table 2. Difference in t_{min} According to Anatomical Locations

Cycle	Location	t_{min} (h)	*P* Value*	Multiple comparison ($P < .05$) †
Day	Cerebral GM	0.5 (0.5–0.5)	.002	Cerebellar WM
	Cerebral WM	1.0 (0.5–1.5)		None
	Cerebellar GM	0.5 (0.5–0.75)		None
	Cerebellar WM	1.25 (0.5–12.0)		Cerebral GM, Putamen
	Putamen	0.5 (0.5–0.5)		Cerebellar WM
Night	Cerebral GM	0.5 (0.5–1.0)	.36	NA
	Cerebral WM	1.0 (0.5–7.0)		
	Cerebellar GM	0.5 (0.5–0.5)		
	Cerebellar WM	0.5 (0.25–12.0)		
	Putamen	0.5 (0.5–0.5)		

Note.—Data are median (interquartile range). GM = gray matter, NA = not applicable, WM = white matter.

* Friedman test

† Wilcoxon test, P values were adjusted for multiple comparisons with the use of Bonferroni correction.

Figure Legends

Figure 1. Flowchart for the study and participant grouping for the crossover design.

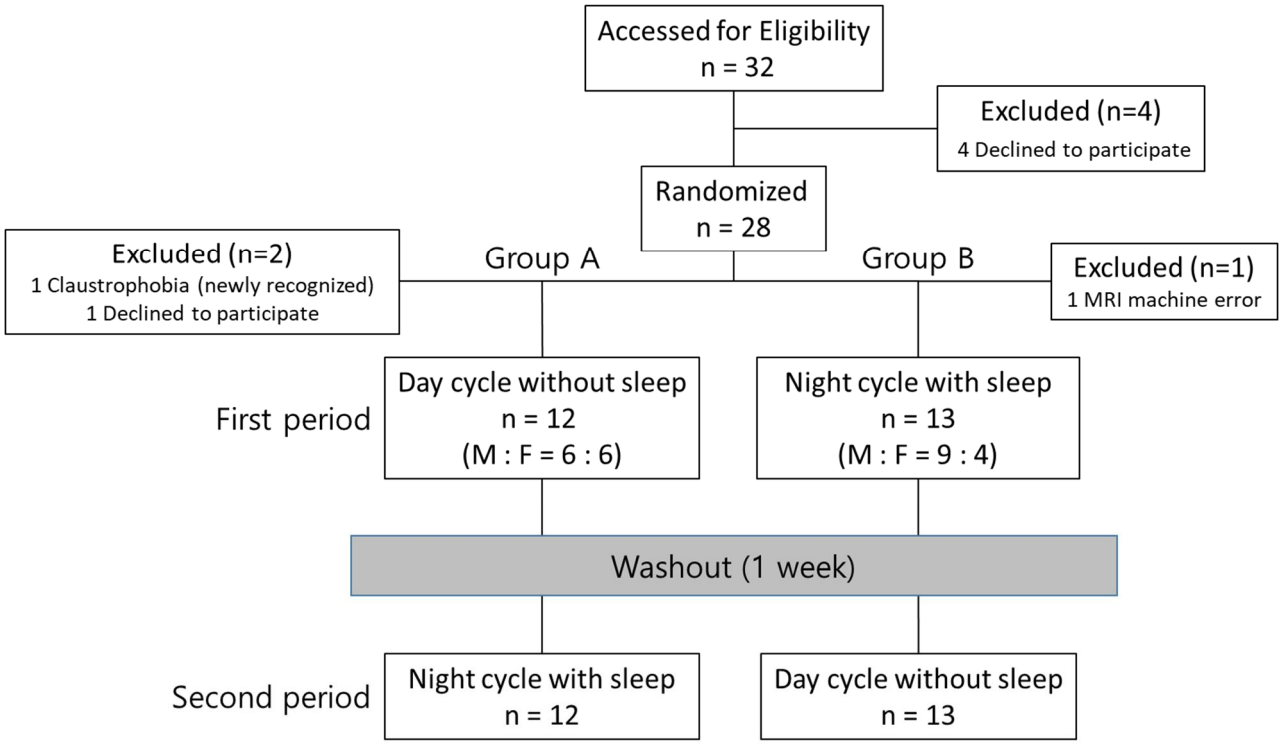

Figure 2. Examples of coregistered anatomical masks on T1 maps.

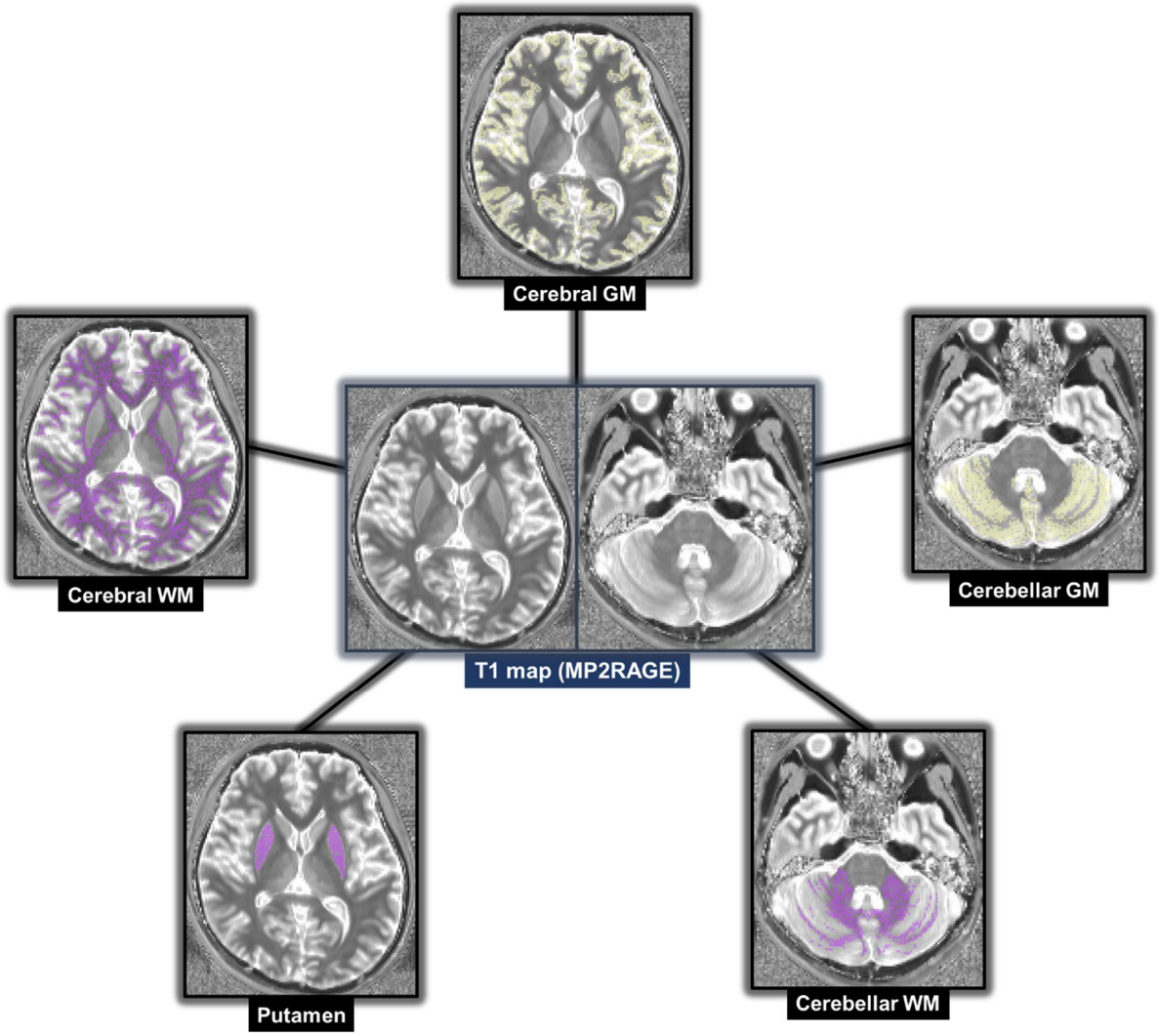

The total volume of interest for each anatomical location is determined through summation of coregistered masks at every slice section.

Figure 3. T1 value-time curves at various anatomical locations.

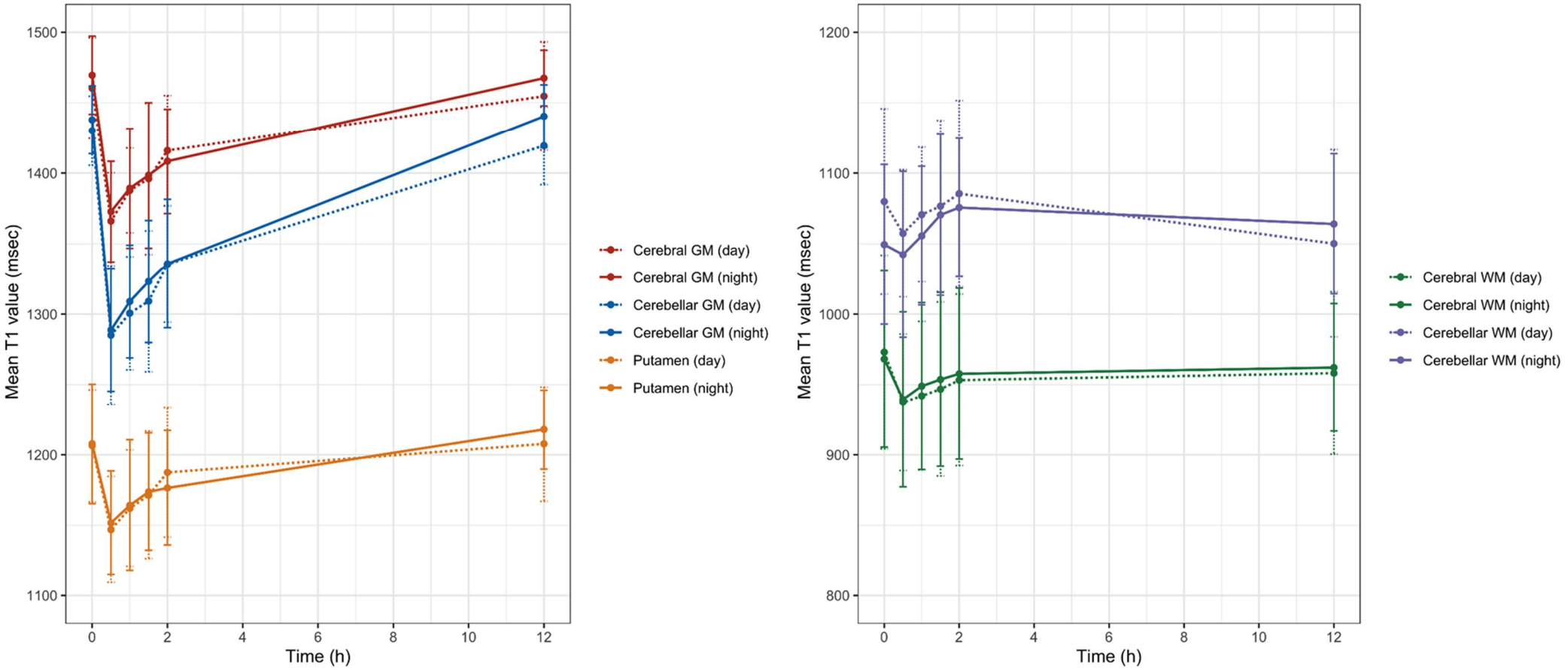

Mean T1 values are shown with standard deviation error bars.

Figure 4. Bar graphs show mean peak ΔT1 according to various anatomical locations in the day (A) and night (B) cycles.

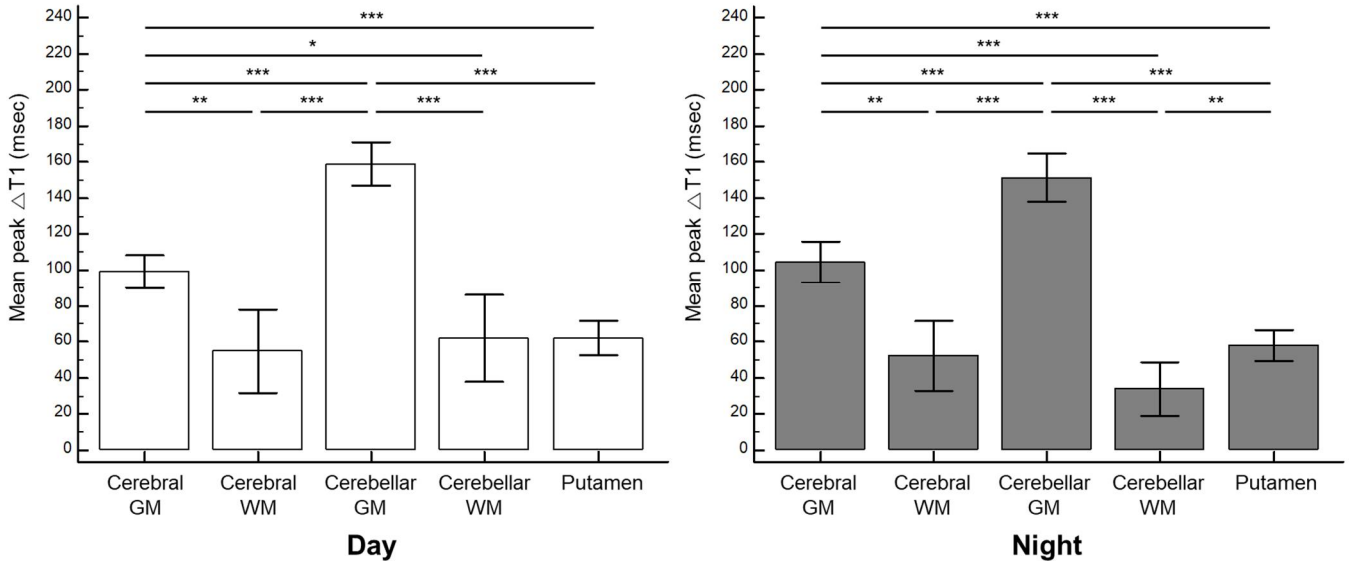

Error bars represent 95% confidence intervals. *P<.05, **P<.01, ***P<.001 (P values for pairwise comparisons without statistically significant difference are not shown.)

Appendix

Appendix E1. *Phantom Calibration Study*

A phantom calibration study was performed to validate the intra-scanner variability of quantitative values calculated from a MP2RAGE sequence. Gadovist 1.0 (Bayer Schering Pharma, Berlin, Germany), a 1.0 mmol/mL solution that contains 604.72 mg of gadobutrol for each milliliter, was prepared for the study. The contrast solution was serially diluted with saline to produce various concentrations as follows: 0, 0.05, 0.08, 0.1, 0.16, 0.20, 0.31, and 0.39 mmol/L. Each diluted contrast solution was filled in 50mL polypropylene Falcon conical tubes, and the tubes were positioned in four rows of two tubes (Fig E1). The temperature of the MRI room was controlled to 20℃. The MP2RAGE sequence was performed four times by using the same protocol shown in Table E1, on a 3.0-T imaging unit (TrioTim, Siemens Healthineers, Erlangen, Germany) with a 32-channel head coil. The tubes were positioned in direction of the B0, along the z-axis in the magnet. A single section image of 4mm thickness was obtained perpendicular to the long axis of the tubes for each scan. T1 relaxation times were calculated by drawing a circular region-of interest (ROI) in the T1 mapping images of the MP2RAGE sequence. The measured T1 relaxation times are described in Table E2. Intraclass correlation coefficient for repeated measurements was excellent (ICC: 0.999, 95% confidence interval [CI]: 0.994 – 1.000).

Table E1. MRI Parameters

Parameter	3D FSPGR	MP2RAGE*
Repetition time (msec)	8.6	5000
Echo time (msec)	2.8	3.64
Flip angle (degree)	9	7, 5 *
Slice thickness (mm)	1.0	2.0
Intersection gap (mm)	0	0
Field of view (mm)	256 x 256	220 x 220
Matrix	256 x 256	200 x 200
Number of excitation	1	1
Scan time	NA	5minutes 4seconds
Inversion time (msec)	NA	700, 1500 *

* MP2RAGE sequence has two gradient echo blocks with different flip angles and inversion times. 3D FSPGR = three-dimensional fast spoiled gradient echo, MP2RAGE = magnetization prepared 2 rapid acquisition gradient echoes sequence.

Table E2. Phantom Calibration Study: T1 values of Gadobutrol Measured with a MP2RAGE Sequence.

Concentration (mmol/L)	T1 value (msec)			
	First acquisition	Second Acquisition	Third acquisition	Fourth acquisition
0.00	2165	2139	2152	2137
0.05	1898	1927	1867	1858
0.08	1491	1518	1467	1455
0.1	1321	1362	1280	1280
0.16	956	964	953	949
0.2	827	835	820	818
0.31	553	563	544	544
0.39	478	495	471	472

Table E3. Pairwise Comparisons of the Peak ΔT1 Values at Different Anatomical Locations.

Cycle	Location pair		Difference in Peak ΔT1	95% Confidence interval*	*P*–value*
Day	Cerebral GM	Cerebral WM	44.52 (11.43)	9.05 ,80.00	0.007
		Putamen	37.11 (6.78)	16.07, 58.16	<.001
		Cerebellar GM	−59.53 (6.46)	−79.59, −39.47	<.001
		Cerebellar WM	37.44 (11.37)	2.14, 72.74	0.03
	Cerebral WM	Cerebral GM	−44.52 (11.43)	−80.00, −9.05	0.007
		Putamen	−7.41 (11.90)	−44.36, 29.54	1
		Cerebellar GM	−10.06 (11.82)	−140.75, −67.36	<.001
		Cerebellar WM	−7.08 (10.10)	−38.43, 24.26	1
	Putamen	Cerebral GM	−37.11 (6.78)	−58.16, −16.07	<.001
		Cerebral WM	7.41 (11.90)	−29.54, 44.36	1
		Cerebellar GM	−96.64 (6.30)	−116.20, −77.09	<.001
		Cerebellar WM	0.33 (10.04)	−30.84, −31.50	1

	Cerebellar GM	Cerebral GM	59.53 (6.46)	39.47, 79.59	<.001
		Cerebral WM	104.06 (11.82)	67.36, 140.75	<.001
		Putamen	96.64 (6.30)	77.09, 116.20	<.001
		Cerebellar WM	96.97 (12.33)	58.69, 135.25	<.001
	Cerebellar WM	Cerebral GM	−37.44 (11.37)	−72.74, −2.14	0.03
		Cerebral WM	7.08 (10.10)	−24.26, 38.43	1
		Putamen	−0.33 (10.04)	−31.50, 30.84	1
		Cerebellar GM	−96.97 (12.33)	−135.25, −58.69	<.001
Night	Cerebral GM	Cerebral WM	52.10 (11.23)	17.24, 86.96	0.001
		Putamen	46.39 (7.10)	24.37, 68.42	<.001
		Cerebellar GM	−47.23 (7.06)	−69.14, 25.32	<.001
		Cerebellar WM	70.44 (9.31)	41.55, 99.33	<.001
	Cerebral WM	Cerebral GM	−52.10 (11.23)	−86.96, −17.24	0.001
		Putamen	−5.70 (10.69)	−38.89, 27.48	1
		Cerebellar GM	−99.33 (10.45)	−131.78, −66.88	<.001

		Cerebellar WM	18.34 (9.71)	−11.81, 48.49	0.72
	Putamen	Cerebral GM	−46.39 (7.10)	−68.42, −24.37	<.001
		Cerebral WM	5.70 (10.69)	−27.48, 38.89	1
		Cerebellar GM	−93.62 (5.49)	−110.67, −76.58	<.001
		Cerebellar WM	24.05 (6.09)	5.13, 42.96	0.006
	Cerebellar GM	Cerebral GM	47.23 (7.06)	25.32, 69.14	<.001
		Cerebral WM	99.33 (10.45)	66.88, 131.78	<.001
		Putamen	93.62 (5.49)	76.58, 110.67	<.001
		Cerebellar WM	117.67 (8.26)	92.04, 143.30	<.001
	Cerebellar WM	Cerebral GM	−70.44 (9.31)	−99.33, −41.55	<.001
		Cerebral WM	−18.34 (9.71)	−48.49, 11.81	0.72
		Putamen	−24.05 (6.09)	−42.96, −5.13	0.006
		Cerebellar GM	−117.67 (8.26)	−143.30, −92.04	<.001

Note.—Data are mean ± standard deviation.

* *P* values were adjusted for multiple comparisons with the use of Bonferroni correction.

Figure E1. Quantitative T1 maps of gadobutrol at various concentrations.

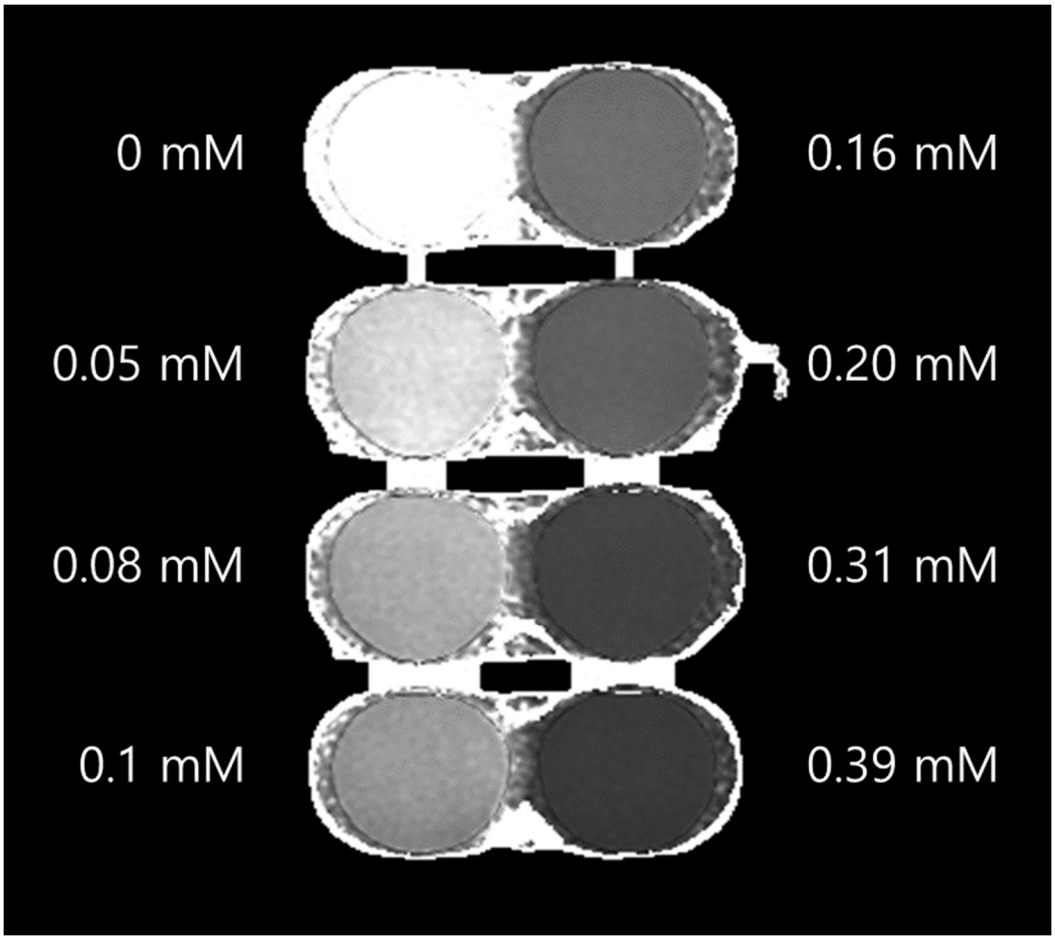

초 록

배경: 글림프계는 신경교세포 의존적 노폐물 제거 경로이며, 야간에 그 활동이 증가한다고 알려져 있다. 척수강내 조영제 주입 후 동적 자기공명영상을 사용한 기존의 글림프계 평가는 임상적 사용이 제한적이다.

목적: 건강한 피험자에서 다양한 해부학적 위치에서의 동적 글림프계 활동의 정량적 평가를 위해 연쇄적 정맥 조영 증강 T1 맵핑을 이용하는 것에 대한 타당성을 평가하고자 한다.

재료 및 방법: 본 무작위, 양방향 교차설계 전향적 연구는 2019년 5월부터 2020년 2월까지 25명의 건강한 20대 참가자 (평균 연령, 24.7세; 범위, 23–29; 남 15명 여 10명)를 대상으로 각각 1주일 간격을 두고 낮과 밤 두 주기의 조영증강 자기공명 영상을 시행하였다. 각 주기마다, 정맥내 조영제 주입 전, 주입 후 30분, 1시간, 1시간 30분, 2시간 그리고 12시간 후 시점마다 자기공명 스캔 (3D T1 강조 영상 및 T1 맵핑)을 수행하였다. 대뇌와 소뇌의 회색질 및 백색질, 그리고 피각에서 T1 값–시간 곡선 상 최소 T1 값 ($T1_{min}$) 에 도달하는 시간 (t_{min}), 조영전 T1 과 $T1_{min}$ 사이의 차이값 (peak ΔT1), 조영제 주입 2시간 후와 12시간 후 측정값들 사이의 기울기 ($slope_{[2h-12h]}$) 를 계산하였다. 수면이 $slope_{[2h-12h]}$ 에 미치는 영향을 평가하기 위해 혼합모형분산분석을 수행하였다. 서로 다른 해부학적 위치간의 t_{min} 과 peak ΔT1을 비교하기 위해 프리드만 검정과 반복측정분산분석을 수행하였다.

결과: 모든 T1 값–시간 곡선은 조영제 주입 후 30분 시점에 초기 감소를 보인 뒤 12시간 후까지 점진적인 회복을 보였다. $Slope_{[2h-12h]}$는 대뇌 회색질, 소뇌 회색질 및 피각에서 낮에 비해 밤에 증가하였으나 (P<.001, 모두) 대뇌 백색질 (P=1.00) 과 소뇌 백

색질 (P=.42) 은 낮과 밤이 차이가 없었다. 대뇌 회색질, 소뇌 회색질, 피각에서 낮밤 주기 모두 t_{min} 중앙값은 30분이었다. Peak ΔT1 은 소뇌 회색질 (평균±표준편차, 158.89 msec ± 5.76 [낮], 151.57 msec ± 6.43 [밤]) 에서 가장 높았고, 그 다음으로 대뇌 회색질 (99.36 msec ± 4.45, 104.34 msec ± 5.46), 피각 (62.25 msec ± 4.64, 57.94 msec ± 4.24) 순이었다.

결론: 연쇄적 정맥 조영 증강 T1 맵핑에서 대뇌/소뇌의 회색질 및 피각의 T1 값 변화는 동적 글림프계 활성도에 대한 잠재적인 영상 생체표지자 역할을 할 수 있을 것이다.

주요어: 글림프계, 정량화, 정맥 조영 증강 T1 매핑, T1 값

학 번: 2018-23561